

Supporting Materials for

Identification the Cr(V)=O Intermediate in Electrocatalytic Water

Oxidation by a Chromium(III)-aqua Complex

Zhi-Kai Shen,^a Zi-Jian Li,^a Zhigang Zou^a and Zhen-Tao Yu^{*a}

^a National Laboratory of Solid State Microstructures and Jiangsu Provincial Key Laboratory for Nanotechnology, College of Engineering and Applied Sciences, Nanjing University, Nanjing, Jiangsu 210093, People's Republic of China.

* Corresponding author: yuzt@nju.edu.cn

Materials

Silver trifluoromethanesulfonate (AgOTf) was obtained from Thermo Scientific Chemicals. Ferrocene was obtained from Alfa Aesar. Tetrabutylammonium hexafluorophosphate and OXONE[®] were obtained from Sigma-Aldrich Lab & Production Materials. Chromous chloride was obtained from aladdin. Ethyl acetate, n-hexane, ammonium chloride, methanol, ethanol, ether, dichloromethane, dry acetonitrile and silver nitrate were purchased from Taicang hushi reagent Co., Ltd. Tetrahydrofuran and n-butyllithium were purchased from J&K Scientific Co., Inc. H₂¹⁸O (97 atom% ¹⁸O) was obtained from MERYER Co., Ltd. All above solvents and reagents were commercially available and used as received without further purification.

Synthesis

The H₂bipyalk ligand was prepared according to previously reported methods.¹ A mixture of chromous chloride (180 mg) and H₂bipyalk (200 mg) in ethanol (40 mL) was stirred at 40 °C for 5 hours. Thereafter, the reaction mixture was cooled down, diffusion of diethyl ether into the reaction mixture gave green single crystals of Cr(H₂bipyalk)(Cl)₃. A mixture of Cr(H₂bipyalk)(Cl)₃ (260 mg) and AgOTf (257 mg) in methanol (40 mL) was stirred at 50 °C for 6 hours. Subsequently, the solvent was removed by rotary evaporation to 1–2 mL, and diethyl ether (20 mL) was added to crystallize at –40 °C. Then, a single crystal Cr complex **1** was obtained. The complex was further recrystallized 3 times for electrochemical analysis.

Measurement apparatus

Single-crystal X-ray diffraction data was obtained at 193 K on a Bruker smart Apex, with Mo K α ($\lambda = 0.71073 \text{ \AA}$) radiation using ω -2 θ scan mode. The data were integrated and scaled using the Bruker-S SAINT software package, and all structures were solved by direct methods and refined on F^2 against full-matrix least-squares methods by using the SHELXTL V 6.12 program package.² Hydrogen atoms were located by geometrical calculation. All non-hydrogen atoms were refined with anisotropic thermal parameters. Crystallographic data are given in Tab. S1. Atmospheric pressure chemical ionization-mass spectrometry (APCI-MS) analysis was performed using a Thermo Scientific Q Exactive Orbitrap. X-ray photoelectron spectroscopy was performed on a Thermo Scientific K-Alpha XPS spectrometer with the binding energies corrected according to C at 284.8 eV. EPR data were collected under an argon atmosphere by Bruker EMX plus 10/12 (equipped with an Oxford ESR910 Liquid Helium cryostat). The UV-vis absorption spectra measurements were performed in 3 mL quartz cells on a PerkinElmer LADBDA950 UV-Vis spectrophotometer. The O₂ produced was determined by using an GC9720Plus Gas Chromatograph. Dynamic light scattering (DLS) was tested by a NanoBrook 90Plus Zeta (Brookhaven, USA). All data was measured 3 times through the system. In situ spectroelectrochemistry was performed using a honeycomb quartz cell ($l = 1 \text{ mm}$) with a Pine 200 electrochemical workstation, where gold honeycomb was used as the working and counter electrode, and a

ferrocenium/ferrocene electrode was used as reference electrode. DEMS measurements were performed on a Hiden HPR-40 mass spectrometer in an online configuration with the electrochemical cell for gas generation analysis. EQCM measurement was run on a CHI 440C EQCM workstation with an Au film-coated quartz crystal as working electrode, a Pt wire counter electrode.

Electrochemical and Catalytic Water Oxidation Testing

Differential pulse voltammetry (DPV) was measured with a GC electrode, $\Delta E = 4$ mV, amplitude = 50 mV, pulse width = 4 s, sampling width = 0.167 s, pulse period = 5 s. The kinetic isotope effect (KIE) was investigated in H₂O and D₂O, respectively. The KIE value was calculated by the following eq. 1.³ The solution was deaerated by bubbling with N₂ gas for 30 min. The onset potential in our manuscript was derived at the intersection point of the potential-axis and the tangent at the maximum slope of the current, that is, calculated by extrapolation to zero current from the linear portion of the J–V curve.⁴

$$KIE = \frac{k_{cat H_2O}}{k_{cat D_2O}} = \left(\frac{i_{cat H_2O}}{i_{cat D_2O}}\right)^2 \dots\dots\dots(1)$$

Determine for Turnover Frequency (TOF)

The value of FOT can be calculated from equations below.^{5,6}

$$i_{cat} = n_{cat} FA[cat]\sqrt{k_{cat}D} \dots\dots\dots(2)$$

$$i_p = 0.4463n_pFA[cat]\sqrt{\frac{n_pFvD}{RT}} \dots\dots\dots(3)$$

$$\frac{i_{cat}}{i_p} = \frac{n_{cat}}{0.4463n_p}\sqrt{\frac{k_{cat}RT}{n_pFv}} \dots\dots\dots(4)$$

In these equations, i_{cat} is the catalytic current, i_p is the peak current, n_{cat} is the number of electrons transferred in water oxidation (4 electrons), n_p is the number of electrons transferred associated with reversible electrochemical couples (1 electron), F is Faraday’s constant, k_{cat} is the pseudo-first-order rate constant, R is the universal gas constant, T is the temperature in kelvin (at a room temperature of 298 K), and v is the scan rate in V/s. The TOF (k_{cat}) can be calculated eq. 5 (simplified from eq. 4).

$$k_{cat} = 0.4847v\left(\frac{i_{cat}}{i_p}\right)^2 \dots\dots\dots(5)$$

Foot of the Wave Analysis (FOWA)

Equations obtained for i/i_p versus $1/\{1+\exp[(E_0-E)F/(RT)]\}$ (WAN, eq. 6) and versus $1/\{1+\exp[(E_0-E)F/(RT)]\}^{3/2}$ (I2M, eq. 7).⁷ Corresponding plots are presented in Fig. 2.

$$\frac{i}{i_p} = \frac{4 \times 2.24 \left(\frac{RT}{Fv} k_{WNA}\right)^{\frac{1}{2}}}{1 + e^{\frac{F(E^0 - E)}{RT}}} \dots\dots\dots(6)$$

$$\frac{i}{i_p} = \frac{4 \times 2.24 \left(\frac{RT}{3Fv} k_D C_{cat}^0\right)^{\frac{1}{2}}}{\left(1 + e^{\frac{F(E^0 - E)}{RT}}\right)^{\frac{3}{2}}} \dots\dots\dots(7)$$

In these equations, F: Faradaic constant; R: gas constant; T: temperature; i : CV current intensity; i_p : peak current intensity of one-electron redox process of the catalyst; E_0 : redox potential obtained by DPV; k_{WNA} : apparent WNA pseudo-rate constant; k_D : apparent dimerization constant.

Calculation Details

All theoretical computations were carried out using Gaussian09 quantum-chemical packages. The full geometric optimizations were performed using the hybrid functional (PBE0)⁸⁻¹⁰ and Grimme dispersion correction.¹¹ The excited state computations were performed using the time-dependent density functional theory (TD-DFT).¹²⁻¹⁴ It was reported that the PBE0 Hybrid functional⁸ gives a better description than the B3LYP functional for the strong correlated system at excitation energy calculation.¹⁵ Therefore the Hybrid PBE0 was used to simulate the *UV-Vis* spectra. The polarized all-electron basis sets at triple-zeta quality (def2-TZVP) developed by Ahlrichs and co-workers were used for the H, C, N, O, and Cr atoms.¹⁶ The free energy were calculated by computing the partition function with consider the vibration, rotation, and translation model of system. The localized orbital bonding analysis (LOBA) for oxidation states determinations were performed using wavefunction analysis software of the Multiwfn.¹⁷

Tab. S1. Summary of the crystallographic and structure data for complex **1**.

| | |
|--|--|
| Empirical formula | C ₁₇ H ₂₂ CrF ₃ N ₂ O ₆ S |
| Formula weight | 491.055 |
| Temperature, K | 193.00 |
| Radiation | MoK α (λ = 0.71073 Å) |
| Crystal system | triclinic |
| Space group | <i>P</i> -1 |
| A (Å) | 9.0515(5) |
| B (Å) | 11.5963(7) |
| C (Å) | 15.9542(9) |
| α (deg) | 70.366(2) |
| β (deg) | 89.852(2) |
| γ (deg) | 81.103(2) |
| Volume (Å ³) | 1556.08(16) |
| Z | 2 |
| Density (g/cm ³) | 1.724 |
| Absorption coefficient (mm ⁻¹) | 0.686 |
| F (000) | 818.0 |
| 2 θ range for data collection | 3.832 to 55.164° |
| Index ranges | -11 \leq <i>h</i> \leq 11, -14 \leq <i>k</i> \leq 15 -17 \leq <i>l</i> \leq 20 |
| Reflections collected | 14757 |
| Independent reflections | 7115 [<i>R</i> _{int} = 0.0373, <i>R</i> _{sigma} = 0.0606] |
| Goodness-of-fit on <i>F</i> ² | 1.069 |
| Data / restraints / parameters | 7115/19/507 |
| Final <i>R</i> indices [<i>I</i> > 2 σ (<i>I</i>)] | <i>R</i> ₁ = 0.0568, <i>wR</i> ₂ = 0.1068 |
| Final <i>R</i> indices (all data) | <i>R</i> ₁ = 0.0872, <i>wR</i> ₂ = 0.1232 |

The crystal structure of complex **1** is available free of charge from the Cambridge Crystallographic Data Centre under reference number CCDC-2408326.

The structure of **1** determined by single crystal X-ray structural analysis is a molecular Cr(III) complex in a distorted square pyramidal coordination environment, which comprises a tetradentate H₂bipyalk as equatorial ligand and a OH₂ and a trifluoromethanesulfonate (OTf) as axial ligands.

Tab. S2. Comparison of Cr–O bond lengths in complex **1** and that in reported complexes.

| Cr–O bond lengths | bond lengths | referenece |
|----------------------------|--------------|------------|
| Cr(III)–OH ₂ | 1.974(2) Å | This work |
| Cr(III)–O(μ -hydroxo) | 1.976(5) Å | 18 |
| Cr(III)–OH ₂ | 2.108(3) Å | 19 |
| Cr(V)–O | 1.604(3) Å | 20 |
| Cr(V)≡O | ca. 1.5 Å | 21 |
| Cr(IV or V)-oxo complexes | 1.49–1.57 Å | 20 |

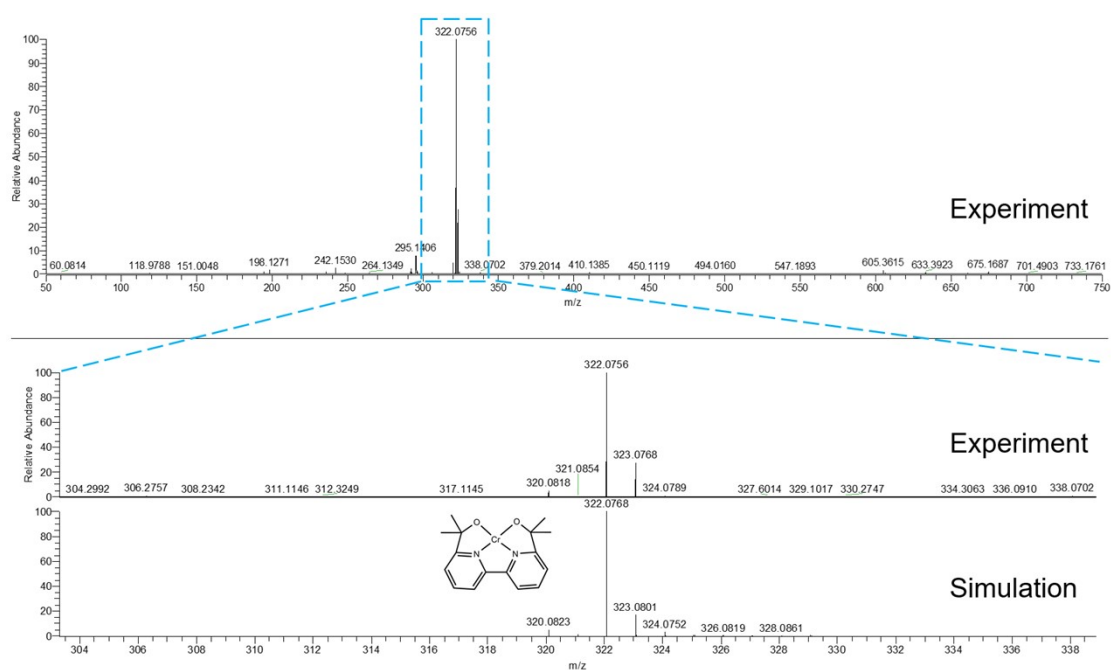


Fig. S1. APCI-MS of complex **1** in MeCN.

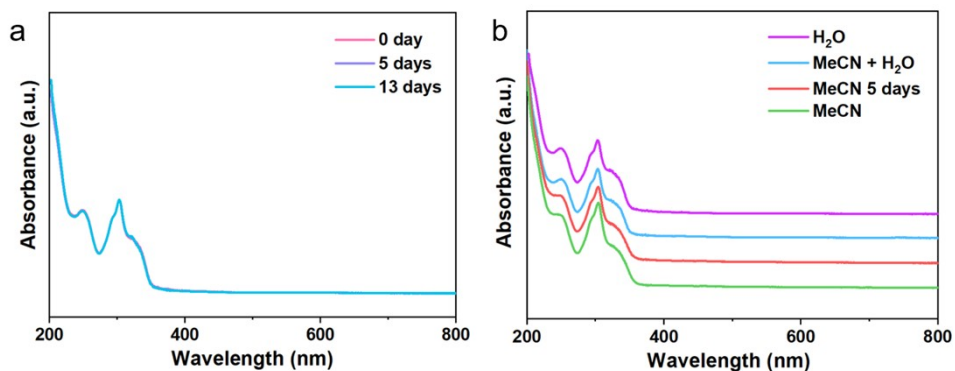


Fig. S2. Time dependent UV-Vis spectra of complex **1** (~ 5 mM) in **a)** aqueous solution, and **b)** acetonitrile solution.

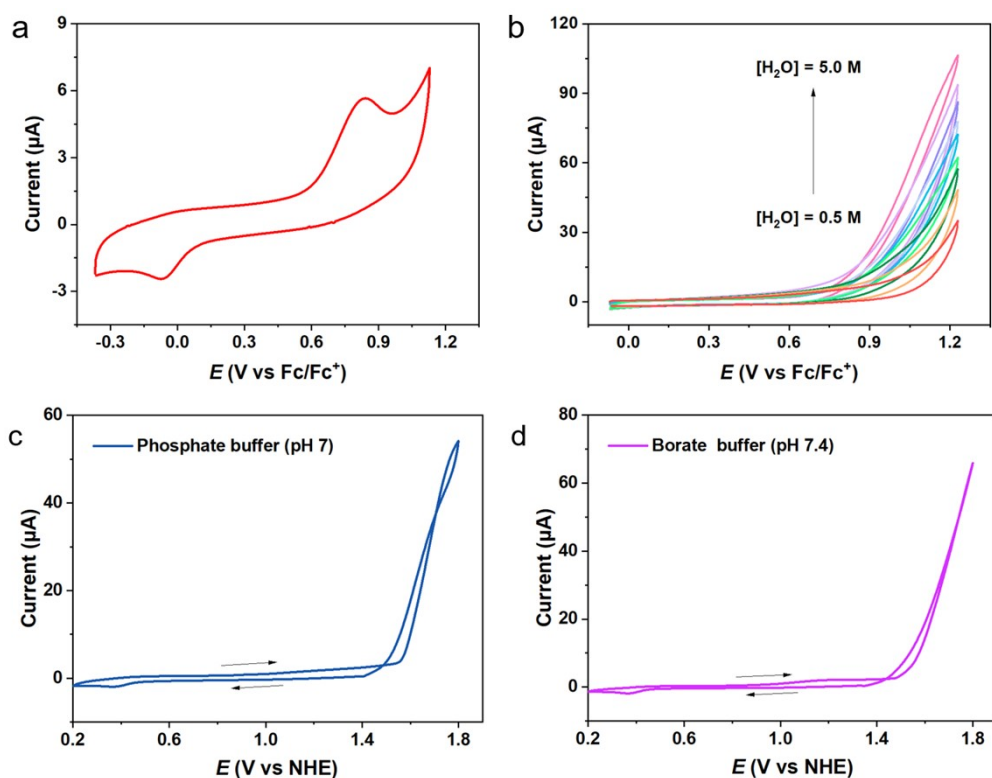


Fig. S3. CVs of 0.5 Mm complex **1** in **a)** acetonitrile solution (0.1 M Et₄NClO₄), and **b)** acetonitrile solution (0.1 M Et₄NClO₄) with various concentration of deionized water. (RDE, GC, 0.2 cm², scan rate, 50 mV s⁻¹, rotating rate, 1600 rpm). CVs of 0.5 mM complex **1** in **c)** phosphate buffer and **d)** borate buffer. The curve-crossing feature of the CV plot likely indicates a heterogeneous catalytic process in buffer solutions.

Tab. S3. Comparison of performance in molecular catalysis for water oxidation.

| complex | onset potential | referenece |
|--|----------------------------------|------------|
| Complex 1 | 0.7 V vs Fc ⁺ /Fc | This work |
| 6-HPACu ₂ (μ-OH)(ClO ₄) ₃ | 1.65 V vs NHE | 22 |
| Co(TCA) ₂ (H ₂ O) ₂ | 1.15 V vs Ag/AgCl | 23 |
| [Fe ^{II} ₄ Fe ^{III} (μ ₃ -O)(μ-L) ₆] ³⁺ | ca. 1.0 V vs Fc ⁺ /Fc | 5 |
| Fe ^{III} (ppq) | 1.25 V vs Ag/AgCl | 24 |
| [Ni(mcp)(H ₂ O) ₂](ClO ₄) ₂ | ca. 1.30 V vs NHE | 25 |
| [Ru ^{IV} (OH)(tda-κ-N ³ O)(py) ₂] ⁺ | 1.3–1.4 V vs NHE | 26 |

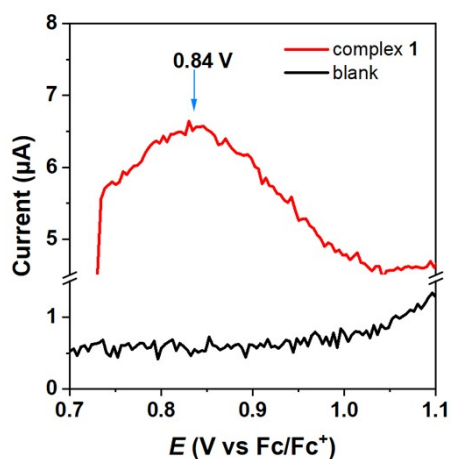


Fig. S4. DPV curve of complex **1** in acetonitrile solutions (0.1 M Et₄NClO₄) with 10 % H₂O.

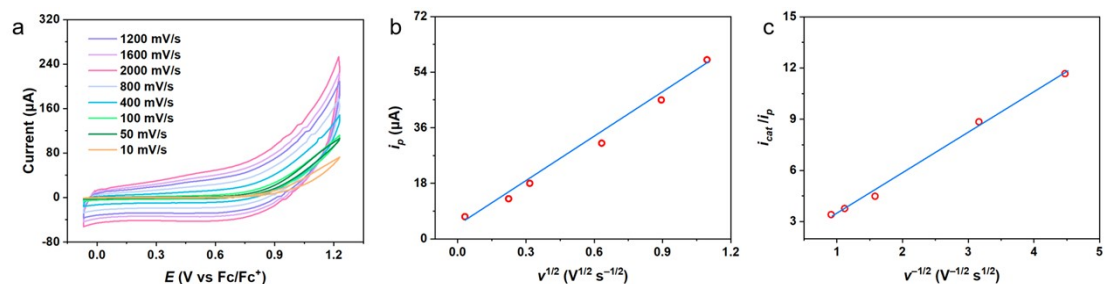


Fig. S5. **a)** CVs of 0.5 mM complex **1** at various scan rates; **b)** Plot of i_p (~ 0.84 V vs Fc^+/Fc determined from DPV) against $v^{1/2}$; **c)** Plot of the ratio of i_{cat} to i_p as a function of the inverse of the square root of the scan rate v . (RDE, GC, 0.2 cm^2 , rotating rate, 1600 rpm).

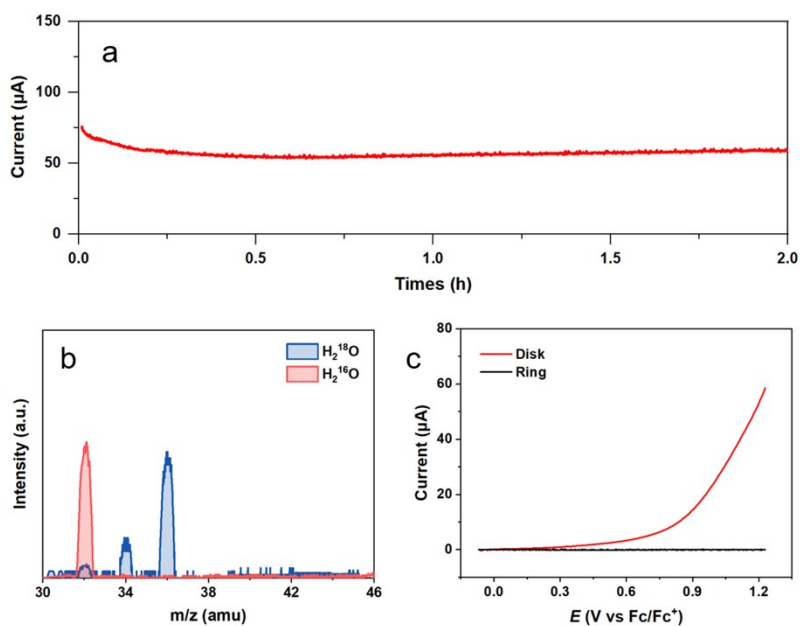


Fig. S6. **a)** Time dependence of electrode current by using FTO (with an exposed area of 1 cm^2) as working electrode at 1.23 V vs Fc^+/Fc with 0.5 mM **1**; **b)** DEMS signals of O_2 products during water oxidation (1.23 V vs Fc^+/Fc) by complex **1** (0.5 mM) in $H_2^{16}O$ or $H_2^{18}O$ (97 atom% ^{18}O)/acetonitrile (1 : 2) mixed solution with 0.1 M Et_4NClO_4 ; **c)** RRDE analysis of 0.5 mM **1** in acetonitrile/ H_2O (10 : 1) mixed solution with 0.1 M Et_4NClO_4 . The rotation rate is 1600 rpm, and the scan rate is 50 mV/s .

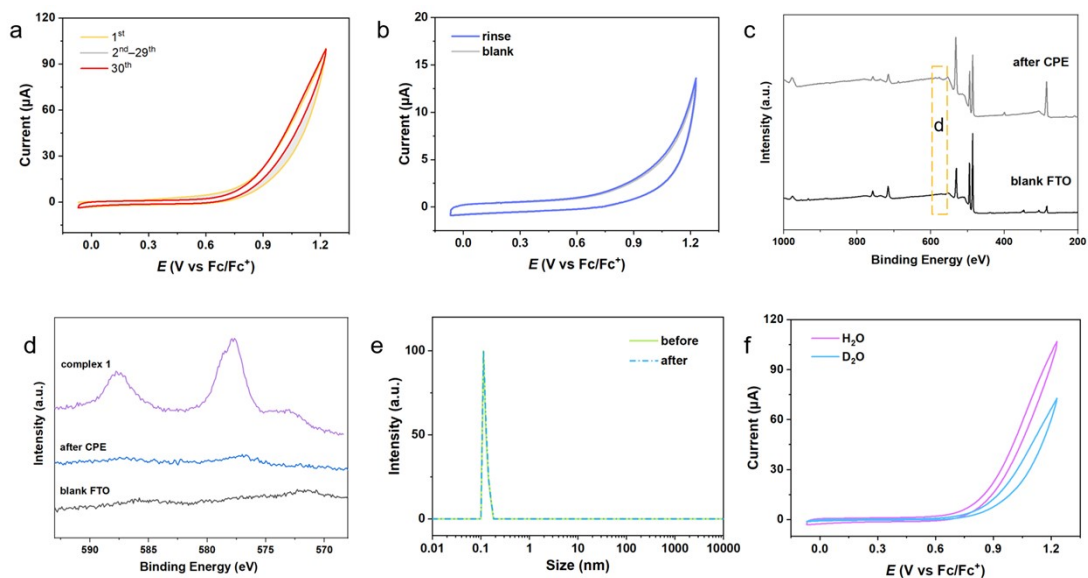


Fig. S7. a) Multiple consecutive CVs of 0.5 mM complex **1** in acetonitrile/H₂O (10 : 1) mixed solution with 0.1 M Et₄NClO₄ (50 mV/s, RDE, GC, 0.2 cm², rotating rate, 1600 rpm); **b)** Blue line: the electrode after 30 scans followed by rinsing and replacement in a fresh background solution; grey line: fresh electrode in a fresh background solution (acetonitrile/H₂O (10 : 1) mixed solution with 0.1 M Et₄NClO₄, 50 mV/s, RDE, GC, 0.2 cm², rotating rate, 1600 rpm). **c, d)** X-ray photoelectron spectroscopy of fresh FTO electrode and after electrolysis under 1.23 V vs Fc⁺/Fc for 2 h. The peak at ca. 688 eV appears after CPE, which corresponding to the F 1s. There may be contamination of F (Organic fluorine) in the system. The peak at ca. 400 eV exists in both samples and represents the N element. **e)** Particle size distribution in electrolyte determined by DLS measurements before and after water oxidation under 1.23 V (vs Fc⁺/Fc) for 2 h; **f)** CVs of 0.5 mM complex **1** in H₂O and in D₂O (a mixed solution of acetonitrile: H₂O (D₂O) = 10:1 with 0.1 M Et₄NClO₄, 50 mV/s, RDE, GC, 0.2 cm², rotating rate, 1600 rpm).

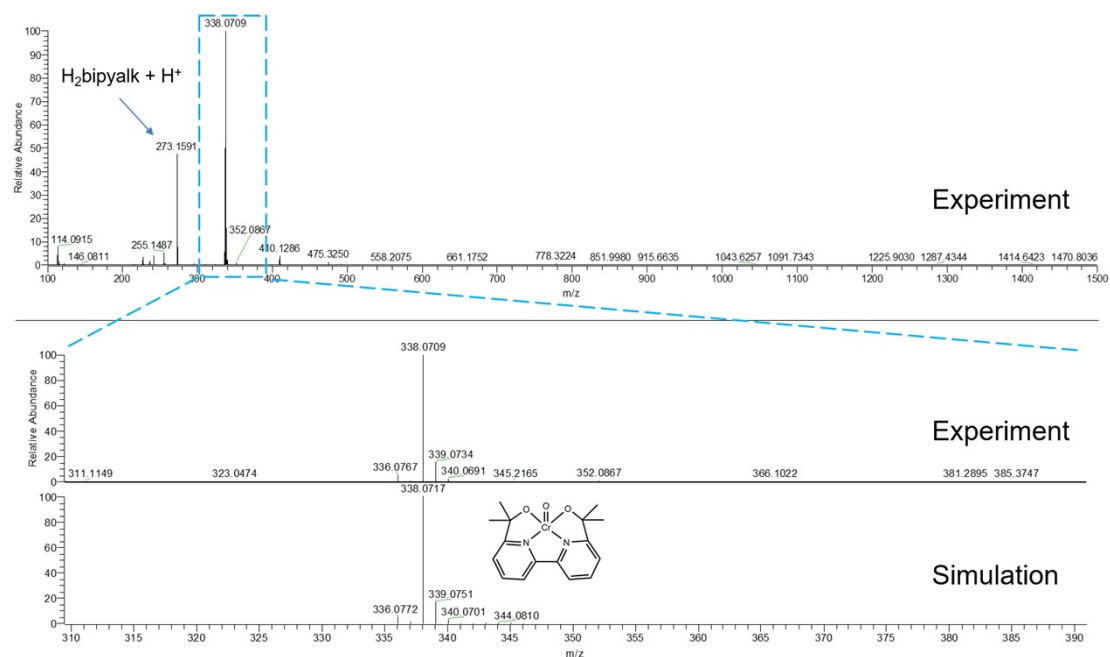


Fig. S8. APCI-MS of complex **1** with 50 equiv. of oxone in MeCN.

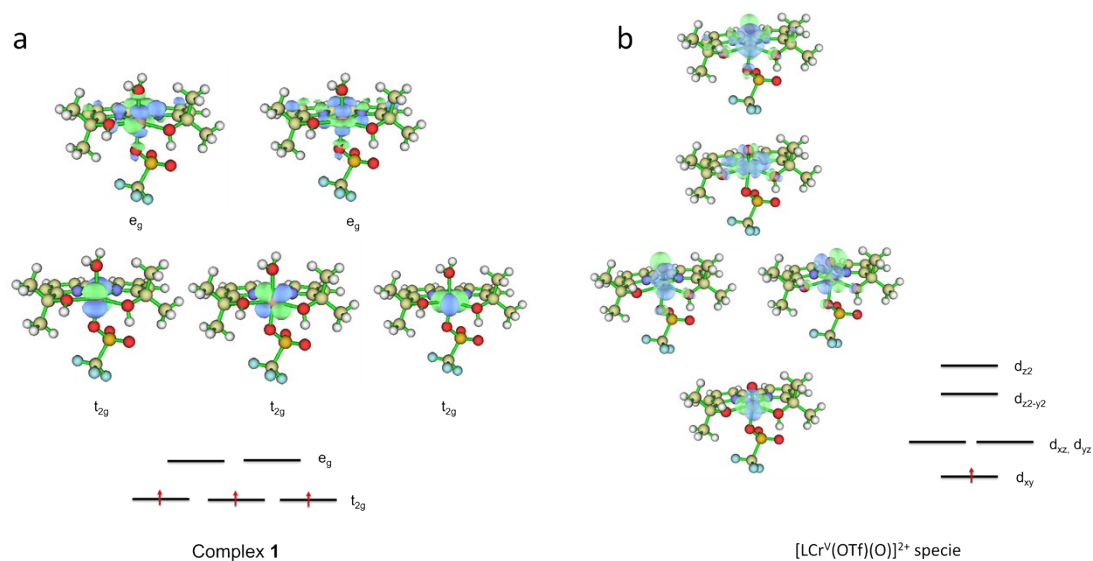


Fig. S9. Electron configuration of 3d electrons in (a) complex **1** and (b) $[\text{LCr}^{\text{V}}(\text{OTf})(\text{O})]^{2+}$ specie. The Cr-3d orbitals contain 3 t_{2g} orbitals and 2 e_g orbitals which are split by the ligand field of complex **1**. The e_g orbitals mixed partial ligand orbitals.

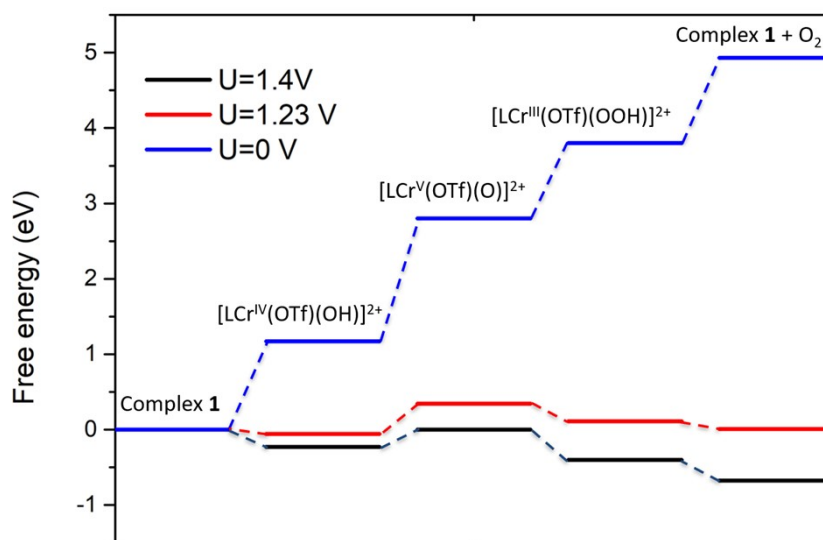


Fig. S10. The free energy diagram of the water oxidation reaction calculated at PBE0/def2-TZVP level, the predicted applied electric potential is 1.4 V, overpotential is less than 0.2 V.

Tab. S4. The spin moment and localized orbital bonding analysis (LOBA) for oxidation states of the Cr during water oxidation cycle.

| species | Complex 1 | [LCr ^{IV} (OTf)(OH)] ²⁺ | [LCr ^V (OTf)(O)] ²⁺ | [LCr ^{III} (OTf)(OOH)] ²⁺ | [LCr ^{III} (OTf)(OO)] ²⁺ |
|----------------------------------|-----------|---|---|---|--|
| Oxidation states | +3 | +4 | +5 | +3 | +3 |
| Spin population | 3.11 | 2.27 | 1.42 | 3.10 | 3.08 |
| Calculated Cr–O bond lengths (Å) | 2.088 | 1.724 | 1.516 | 2.076 | 2.294 |

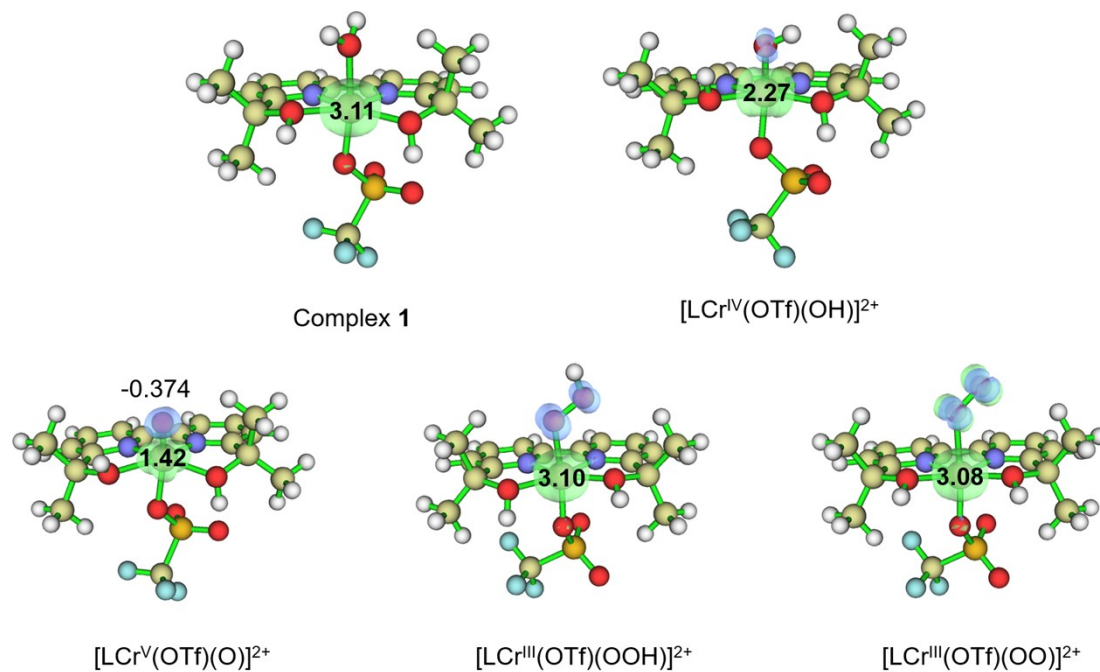


Fig. S11. The spin moment of the Cr during water oxidation cycle.

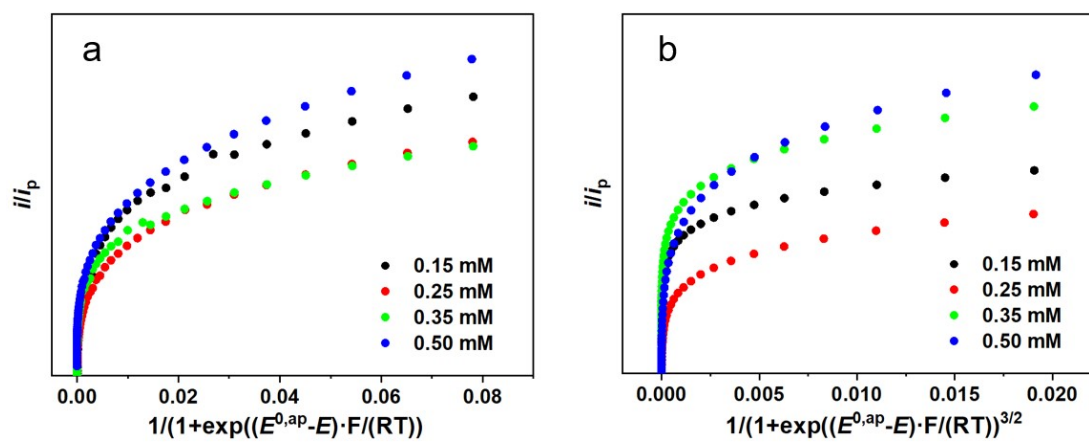


Fig. S12. **a)** i/i_p vs $1/\{1+\exp[(E^0-E)F/(RT)]\}$ plots under different catalyst concentration assuming a WNA mechanism, **b)** i/i_p vs $1/\{1+\exp[(E^0-E)F/(RT)]\}^{3/2}$ plots under different catalyst concentration assuming a I2M mechanism. The original CVs are shown in Fig. 2b.

Reference

- 1 B. Rudshiteyn, K. J. Fisher, H. M. C. Lant, K. R. Yang, B. Q. Mercado, G. W. Brudvig, R. H. Crabtree and V. S. Batista, *ACS Catal.*, 2018, **8**, 7952–7960.
- 2 G. M. Sheldrick, *Acta Crystallogr. Sect. A*, 2008, **64**, 112–122.
- 3 W. Guo, Z. Shen, Y. Su, K. Li, W. Lin, G. Chen, J. Guan, X. Wang, Z. Li, Z. Yu and Z. Zou, *Dalton Trans.*, 2022, **51**, 12494–12501.
- 4 J. Xie, P. Yang, C. Tang, T. Chen, C. Zhong, L. Wang and Y. Huang, *Adv. Mater. Interfaces*, 2021, **8**, 2101069.
- 5 M. Okamura, M. Kondo, R. Kuga, Y. Kurashige, T. Yanai, S. Hayami, V. K. K. Praneeth, M. Yoshida, K. Yoneda, S. Kawata and S. Masaoka, *Nature*, 2016, **530**, 465–468.
- 6 K. G. Kottrup, S. D'Agostini, P. H. van Langevelde, M. A. Siegler and D. G. H. Hetterscheid, *ACS Catal.*, 2018, **8**, 1052–1061.
- 7 R. Matheu, S. Neudeck, F. Meyer, X. Sala and A. Llobet, *ChemSusChem*, 2016, **9**, 3361–3369.
- 8 C. Adamo and V. Barone, *J. Chem. Phys.*, 1999, **110**, 6158–6170.
- 9 J. P. Perdew, *Phys. Rev. B*, 1986, **33**, 8822–8824.
- 10 J. P. Perdew, K. Burke and M. Ernzerhof, *Phys. Rev. Lett.*, 1996, **77**, 3865–3868.
- 11 S. Grimme, S. Ehrlich and L. Goerigk, *J. Comput. Chem.*, 2011, **32**, 1456–1465.
- 12 R. Bauernschmitt, M. Häser, O. Treutler and R. Ahlrichs, *Chem. Phys. Lett.*, 1997, **264**, 573–578.
- 13 E. Runge and E. K. U. Gross, *Phys. Rev. Lett.*, 1984, **52**, 997–1000.
- 14 R. E. Stratmann, G. E. Scuseria and M. J. Frisch, *J. Chem. Phys.*, 1998, **109**, 8218–8224.
- 15 C.-X. Wang, Y. Li, Z.-F. Li, Z.-J. Liu, E. F. Valeev and L. V. Moskaleva, *J. Phys. Chem. A*, 2020, **124**, 82–89.
- 16 F. Weigend and R. Ahlrichs, *Phys. Chem. Chem. Phys.*, 2005, **7**, 3297.
- 17 T. Lu and F. Chen, *J. Comput. Chem.*, 2012, **33**, 580–592.
- 18 M. P. Donzello, L. Bartolino, C. Ercolani and C. Rizzoli, *Inorg. Chem.*, 2006, **45**, 6988–6995.
- 19 S. L. Hooe, J. M. Dressel, D. A. Dickie and C. W. Machan, *ACS Catal.*, 2020, **10**, 1146–1151.
- 20 J. Cho, J. Woo, J. Eun Han, M. Kubo, T. Ogura and W. Nam, *Chem. Sci.*, 2011, **2**, 2057.
- 21 H. Kotani, S. Kaida, T. Ishizuka, K. Mieda, M. Sakaguchi, T. Ogura, Y. Shiota, K. Yoshizawa and T. Kojima, *Inorg. Chem.*, 2018, **57**, 13929–13936.
- 22 Q. Chen, K. Xian, H. Zhang, X. Su, R. Liao and M. Zhang, *Angew. Chem. Int. Ed.*, 2024, **63**, e202317514.
- 23 H. A. Younus, N. Ahmad, A. H. Chughtai, M. Vandichel, M. Busch, K. Van Hecke, M. Yusubov, S. Song and F. Verpoort, *ChemSusChem*, 2017, **10**, 862–875.
- 24 L. D. Wickramasinghe, R. Zhou, R. Zong, P. Vo, K. J. Gagnon and R. P. Thummel, *J. Am. Chem. Soc.*, 2015, **137**, 13260–13263.
- 25 J. Wang, X. Zhang, H. Huang and T. Lu, *ChemCatChem*, 2016, **8**, 3287–3293.
- 26 R. Matheu, M. Z. Ertem, J. Benet-Buchholz, E. Coronado, V. S. Batista, X. Sala and A. Llobet, *J. Am. Chem. Soc.*, 2015, **137**, 10786–10795.

